Journal of Molecular Structure 1202 (2020) 127236

Contents lists available at ScienceDirect

Journal of Molecular Structure

journal homepage: http://www.elsevier.com/locate/molstruc

Properties of fly ash-based lightweight geopolymer concrete prepared using pumice and expanded perlite as aggregates

Soner Top [a, *], Hüseyin Vapur [b], Mahmut Altiner [b], Dogan Kaya [c], Ahmet Ekicibil [d]

[a] Materials Science and Nanotechnology Engineering Department, Abdullah Gül University, Kayseri, 38080, Turkey
[b] Mining Engineering Department, Cukurova University, Adana, 01330, Turkey
[c] Department of Electronics and Automation, Vocational School of Adana, Cukurova University, 01160, Cukurova, Adana, Turkey
[d] Department of Physics, Cukurova University, Adana, 01330, Turkey

ARTICLE INFO

Article history:
Received 15 March 2019
Received in revised form
17 September 2019
Accepted 14 October 2019
Available online 16 October 2019

Keywords:
Geopolymer
Fly ash
Lightweight
Perlite
Pumice
Aggregate

ABSTRACT

The present paper aims to utilize the fly ash wastes with lightweight aggregates for geopolymer concrete production process in which sodium hydroxide (NaOH) and sodium metasilicate (Na_2SiO_3) were used as alkali activators, respectively. The designed experiments were examined by the Yates Analyses and so the productions of geopolymer concrete were investigated depending on curing temperature, solid/liquid rate and concentration of alkali activators. The curing temperature and alkali activator concentration were revealed as effective parameters in geopolymerization. The effects of expanded perlite (EP) and acidic pumice (AP) aggregates were discovered for the production of lightweight geopolymer concretes. The microstructural properties of each produced geopolymer concrete were characterized using SEM, EDS and laser particle size analyses. The specifications of the concrete were evaluated based on their uniaxial compressive strength (UCS), point load strength (PLS), sonic speed (SS), Mohs hardness (MH), and water absorption (WAR) ratio results. In addition, the effects of pre-wetting of EP aggregates, which have hydrophilic nature, were examined. To the best of our knowledge, this is the first time that pre-wetted lightweight EP aggregates were used to produce lightweight GP concretes. As a result of pre-wetting, chemical usage decreased by 32.5%. The UCSs of the lightweight geopolymer concretes were in a range of 10–50 MPa and their unit weights changed between 1250 and 1700 kg/m^3. Lighter concretes were obtained by the addition of EP aggregates rather than AP ones.

1. Introduction

Geopolymer (GP) is the most promising advanced material that substituted the traditional portland cement (PC) and can be used in bottom-up all fields of industry applications [1–3]. It is well known that the PC is responsible for about 5–7% of CO_2 emissions caused by human being [4,5]. During the PC production, CO_2 emissions are generated not only by calcination during clinker production but also by using fossil fuels to provide calcination temperature. Both of them are equally responsible for CO_2 emissions [6]. GP has numerous advantages such as fireproof, environmental sensitivity, low price, and permeability, in comparison with the PC [7,8].

GP, which was introduced by Davidovits for the first time [9], consists of AlO_4 and SiO_4 tetrahedrals creating poly(sialate), poly(sialate-siloxo) and poly(sialate-disiloxo) molecular structures to form three-dimensional polymeric chains [10]. Geopolymerization reaction occurs between solid aluminosilicate oxides (minerals or inorganic by-products) and alkali metal silicate solutions (NaOH, KOH, etc.) to build amorphous or semi-crystalline polymeric constructs containing Si–O–Si and Si–O–Al frameworks in high alkali conditions and at moderate temperatures (20–150 °C) [11]. The empirical formula of GPs is as follow:

$$Xq\,[-(SiO_2)a-AlO_2]q.nH_2O \quad (1)$$

where X is a metal cation (Ca^{2+}, K^+ or Na^+), a is 1, 2 or 3, and q is the polycondensation degree.

Many materials such as fly ash [12], metakaolin [13], glass waste [14], red mud [15], ashes of the agriculture industry by-products (coconut, bagasse, rice husk, etc.) [16–18], ferrochrome slag [19], and concrete demolition waste [20] have been used to produce GP concrete due to their high aluminosilicate contents.

* Corresponding author.
E-mail address: soner.top@agu.edu.tr (S. Top).

https://doi.org/10.1016/j.molstruc.2019.127236
0022-2860/

Lightweight concretes, which have a density less than 1920 kg/m^3, offer remarkable advantages in terms of the dead load reducing, easy transportation, and developed thermal and sound insulations [21,22]. Huang et al. have compared the microstructure features between lightweight and normal-weight concretes in their recent study [23]. They have pointed out that the bond between lightweight aggregate and cement paste is relatively tight, and there are no visible cracks at the joint interface. Lightweight concrete has an anti-earthquake effect compared to portland cemented concretes because the reduction of vertical forces results in a decrease in inertia affecting the structure [24]. Yasar et al. have produced lightweight concrete, which reduces the seismic risk, from a mixture of fly ash, silica fume and scoria [25]. Lightweight concretes are mostly prepared by adding the lightweight aggregates, typically volcanic rocks such as pumice, scoria, and vermiculite, into mortar [26–29]. Foamed plastics, sintered clay minerals, and exfoliated vermiculites are also used as low-density aggregates [30–32]. Likewise, they can be produced for special purposes under different trade names and chemical compositions [33,34].

One of the most important problems encountered in concretes formed by using lightweight aggregates is their high water absorption capacity. This problem can be overcome by pre-wetting lightweight aggregates. It has been stated in previous studies that concrete samples obtained by using pre-wetted lightweight aggregates may have higher strength [35,36].

In this study, fly ash-based GP concretes were prepared by adding AP and expanded perlite (EP) aggregates. The best geopolymerization conditions were revealed after Yates Analyses. Sodium hydroxide (NaOH) and sodium silicate (Na_2SiO_3) solutions were used to determine convenient alkali reagent, separately. Pre-wetting of EP aggregates, which has not been studied before for GP concretes, and their effects on the material properties of GP concrete specimens were examined. In addition, the effects of aggregate grain sizes were investigated in detail.

2. Experimental

2.1. Materials

Class F fly ashes (according to ASTM C618-17a) were taken from Sugözü thermal power station located in southern Anatolia [37]. Pumice samples were obtained from a mine in Nevsehir province of Turkey while EP samples were purchased from Akper Company located in central Anatolia. The chemical compositions of the samples were detected by XRF (Minipal 4) analysis (see Table 1).

X-ray diffraction (XRD) patterns of each sample were obtained using a Rigaku Miniflex XRD equipped with a Cu Ka radiation in the 2ø range of 5–75° and the material phases were identified through a PDXL software using the current database. XRD patterns of the samples are given in Fig. 1 for fly ash (black), AP (red), EP (blue) and peaks revealed that all the materials had amorphous silica which had confirmed by a broad peak between 15 and 45°. The crystalline phases were determined as quartz (Q: SiO_2) and mullite (M: $Al_6Si_2O_{13}$) minerals in fly ash while only quartz mineral was detected in pumice. However, EP sample was composed entirely of amorphous silica as seen in Fig. 1c.

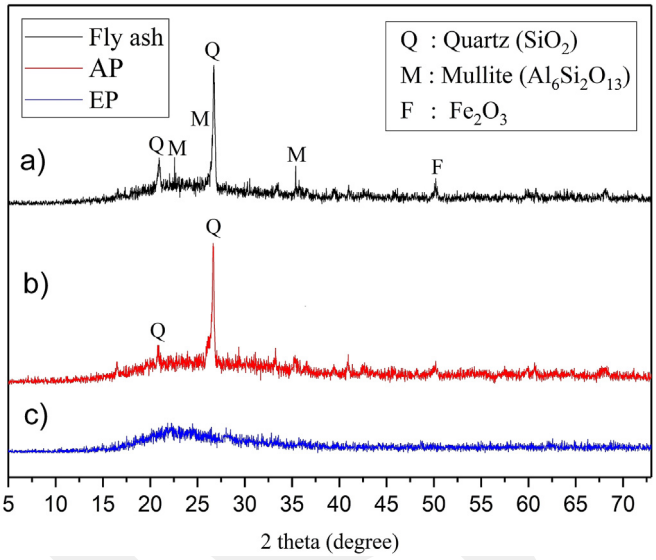

Fig. 1. XRD patterns of the samples. (a) XRD pattern of Fly ash, (b) XRD pattern of AP, and (c) XRD pattern of EP aggregates with major peaks of Q: Quartz (SiO_2), M: Mullite $Al_6Si_2O_{13}$, F: Fe_2O_3.

The morphological structures of the samples were analysed by Quanta FEG 650 scanning electron microscope (SEM) and presented in Fig. 2(a–c) fly ash, AP and EP, respectively. SEM images revealed that the fly ash samples formed spherical structures. SEM micrographs of EP showed that a typical porous foamy structure with broken ragged edges were in good agreement with the previous findings [38,39]. The glassy and broken surface morphologies that were similar to both the EP and the previous studies [40,41] were seen in the pumice samples.

The particle size distribution of fly ash, AP, and EP samples are given in Fig. 3. Here, the pumice samples were crushed with a laboratory scale jaw crusher. The size distribution of pumice samples (−12 mm) were provided to be compatible with TS 802 (Turkish concrete mixture design standard) [42]. The d_{50} value was 1.20 mm for EP and 1.50 mm for pumice using a dry sieving analysis, while the d_{50} value of fly ash sample was found to be 8.75 μm using a BT 9300 HT laser analyser.

2.2. Methods

NaOH or Na_2SiO_3 solutions were used to provide geopolymerization and additional water was not added to the mortar. The chemicals used without any purification in this study [sodium metasilicate (Na_2SiO_3) and sodium hydroxide (NaOH)] were supplied from TEKKIM Co. Tap water was used for the alkali solution preparation. The mortar was composed of fly ash, an alkali solution, and lightweight aggregates. The mixture was manually stirred for 5 min before pouring into molds. Afterward, the mortar was poured into $50 \times 50 \times 50$ mm^3 molds conforming to ASTM C109/C109M-16a testing standards [43]. The molds were shaken for 3 min to remove any air trapped inside the mortars. After approximate

Table 1
Chemical analysis of the fly ash, AP, and EP samples.

Sample	SiO_2	Al_2O_3	CaO	Fe_2O_3	K_2O	SrO	TiO_2	BaO	Na_2O	SO_3	LOI
Fly ash	55.20	24.10	5.50	8.11	1.62	0.27	1.44	0.24	*	0.72	2.34
AP	69.70	13.64	3.15	2.34	4.07	0.03	0.15	*	0.40	0.07	3.65
EP	75.16	14.50	1.01	1.04	5.98	0.03	0.14	0.10	*	*	1.35

*Below detection limit.

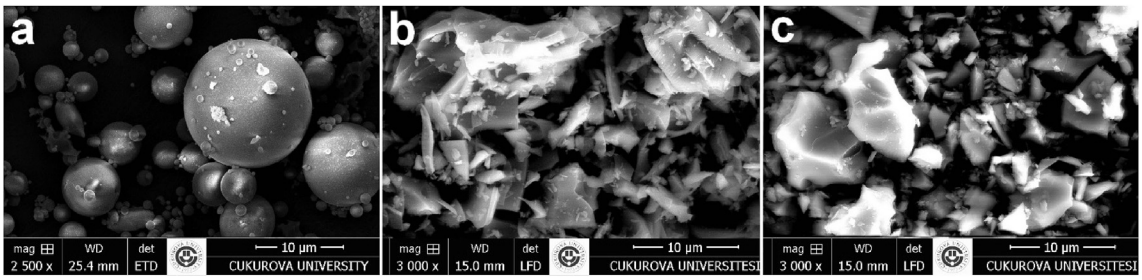

Fig. 2. SEM micrographs of the samples: a) Fly ash, b) AP, c) EP.

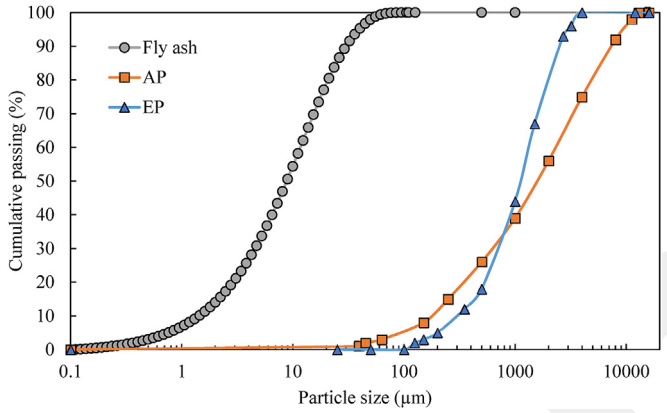

Fig. 3. Particle size distributions of the samples, Fly ash, AP, EP (logarithmic scale).

1.5–2 h, which was enough for the solidification of mortars, the specimens were demolded. When higher temperature (>20 °C) curing was applied, the samples were placed in the oven for 24 h. The curing process was then continued at room temperature. The compressive strengths of the specimens were measured on the 1st, 5th, 10th, 15th, and 28th days with a uniaxial compressive strength (UCS) device (ELE). The pressure increase in the device was chosen to be 0.50 MPa per second and it was applied until the specimens were broken. The value at which the specimen breaks was recorded as the UCS. In addition, the PLS, WAR, and SS values of the mortar were determined according to ASTM C1245/C1245M – 12 [44], ASTM C642–13 [45], and ASTM C597-16 [46], respectively.

The relative humidity values were between 45 and 60% during the curing periods. The MH value of each specimen was determined using a shore scleroscope, which measures the hardness by taking advantage of the elasticity of the material [47]. The stress-strain curves were graphed to reveal the concrete behaviors under pressure using the following formula:

$$E = \frac{\frac{F}{A}}{\frac{dx}{d0}}, \quad (2)$$

where F is the force (N), A is area (mm^2), dx is the length change in the specimen (m), d0 is the initial length of the specimen (m), and E is Young's modulus (MPa).

The experiments were designed based on the 2^n factorial experimental approach, which is the application of the least number of experiments with multiple variables at the same time. Then the responses were evaluated by Yates Analyses to reveal the effect of variables on strengths. In the 2^n factorial design, because only 2^n of experiments are required, the test conditions must be given with a special notation and sorting [48]. This is called Yates arrangement of notation. Yates Analysis is a methodical approach

Table 2
Test design for Yates Analysis.

Test symbol	A: Curing temperature	B: Solid/liquid ratio	C: Concentration of the solution
1	50	72	3
A	70	72	3
B	50	76	3
AB	70	76	3
C	50	72	5
AC	70	72	5
BC	50	76	5
ABC	70	76	5
Mean	60	74	4

applied to find out the principle and interior interactions of the 2^n factorial design [49]. Firstly, the concrete specimens were produced from fly ash and alkaline solutions to determine the more realistic experimental parameters. Afterward it was aimed to produce lightweight concrete with the use of lightweight pumice and EP aggregates according to the results obtained by Yates Analysis. Table 2 listed the experimental conditions in the study. A (X_1): Curing temperature (°C), B (X_2): solid/liquid ratio by weight (%), and C (X_3): molarity of the alkali solutions (M) were selected as variables (2^3 factorial, n = 3). For example, the notation of AB indicates that the experiment was performed under the following conditions: curing temperature of 70 °C, solid/liquid ratio of 76%, and 3 M of alkali solution. The temperature curing time of 24 h was kept constant for all the tests. The whole test design was applied separately for NaOH and Na_2SiO_3 solutions.

3. Results and discussions

3.1. Evaluation of experimental results based on Yates Analyses

Firstly, the preliminary tests were performed and the high and low levels for Yates Analyses were determined. The effects of the alkaline solution nature, solid/liquid ratio and the curing temperature on UCSs of the produced GP concretes were investigated using the Yates Analysis. Concretes were produced in 8 different conditions for each Yates Analysis and the strength tests of the samples were carried out on 1st, 5th, 10th, 15th and 28th days. The obtained UCSs were taken as responses (observed values) for Yates Analysis. Besides, 3 GP concretes produced by mean experimental condition were tested to calculate the sample variance (Se^2). For the experiments using NaOH and Na_2SiO_3, 10 Yates table (for 1st, 5th, 10th, 15th and 28th day strengths) were created. The Yates Analysis results, in which the highest UCS was measured, were given in Table 3. The other analysis results were given in the Appendix. In the tables, the values in the "data" column are divided into pairs, respectively. In column I^a, these pairs were first collected in sequence and half of the column continued with these collections.

Table 3
Yates Analysis results for 28th day (in Na_2SiO_3 solution).

Yates Notation	Data	I[a]	II[a]	TE[a]	$(TE)^2/2^3$	DF[b]	Fvalue[c]	Ftable	Decision	Y[d]
1	10.98	39.92	83.15	227.85						11.58
A	28.93	43.22	144.70	69.813	609.24	1	135.55	5.32	Active	29.52
B	14.25	67.13	32.66	13.73	23.59	1	5.24	5.32	Passive	12.06
AB	28.96	77.57	37.14	2.95	1.08	1	0.24	5.32	Passive	29.52
C	25.83	17.95	3.30	61.55	473.64	1	105.38	5.32	Active	27.44
AC	41.30	14.70	10.43	4.48	2.51	1	0.55	5.32	Passive	44.90
BC	27.94	15.47	−3.24	7.12	6.35	1	1.41	5.32	Passive	27.44
ABC	49.62	21.67	6.19	9.44	11.14	1	2.48	5.32	Passive	44.90

The average of mean experiments was 11.18 MPa.
[a] Yates calculations (for n = 3 factor).
[b] Degrees of freedom.
[c] $[(TE)^2/2^3]/(DF^*Se^2)$ [here; TE is total effect and Se is standard error].
[d] Response values obtained from the formula.

The other half of the column was completed by subtracting the values below from the top values. These operations were also continued for columns II[a] and TE[a]. The other calculations of columns were given as footnote below the tables. The F_{table} value is a fixed value determined by the 95% confidence interval. The calculated F_{value} value was compared with the F_{table} value to determine whether the variables or the interactions of the variables were effective or ineffective. It was clear that temperature and alkaline solution concentration were predominant parameters as A and C variables were found to be effective in all Yates Analyses. Due to the low sensitivity of the device, the UCSs of some samples on 1st and 5th days could not be measured.

Using the test results in Table 3, Equation (3) that characterizes the UCSs of GP concretes was created. The predicted UCS values based on the experimental parameters were calculated by the formula given below.

$$y = 28.48 + 8.73X_1 + 7.69X_3 \quad (3)$$

As seen in Fig. 4, there are strong correlations (R^2) between the real and calculated values. The UCSs of the concretes prepared with NaOH did not exceed 20 MPa, but the concretes prepared with Na_2SiO_3 reached up to 47 MPa strength. Yahya et al. [50] stated that increasing the Na_2SiO_3 amount increased the dissolution rate of aluminasilicate source material used for geopolymerization. Xu and Van Deventer [51] also indicated that Na_2SiO_3 usage accelerated the geopolymerization process and improved the UCS values. Therefore, it was decided to use Na_2SiO_3 solution as the alkaline activator in the next experiments in the light of experimental findings.

The 28th day GP concrete produced at the condition of ABC (with Na_2SiO_3) was ground to be evaluated in SEM examination, which was given in Fig. 5a. It is clearly seen in Fig. 5a that polysialate structures and their derivatives were detected on a fly ash sphere. Furthermore, the EDS spectrum of the area revealed that Na doping derived due to the use of Na_2SiO_3 was obvious (see Fig. 5b).

3.2. Effects of curing temperature and Na_2SiO_3 concentration

The effects of these factors on the UCS values of concrete were investigated in detail because the curing temperature and Na_2SiO_3 concentration have the strongest effects on UCSs based on the Yates Analysis. The effect of the curing temperature and Na_2SiO_3 concentration on the UCS values of concrete were investigated in detail using the Yates Analysis.

Our experiments carried out with mortars prepared at a solid rate of 74%, the strengths of the concrete samples that were kept in the oven at 70 °C for 24 h and were compared with the other concrete samples cured in room temperature, simultaneously. The molarity of solution was 5 M. Fig. 6 shows the comparison of the UCS and unit weight values of concrete cured at 70 °C (orange) and room temperature (green), respectively. It is clearly understood from Fig. 6 that the curing temperature played a crucial role in the strength property of concrete and led to a decrease in its curing

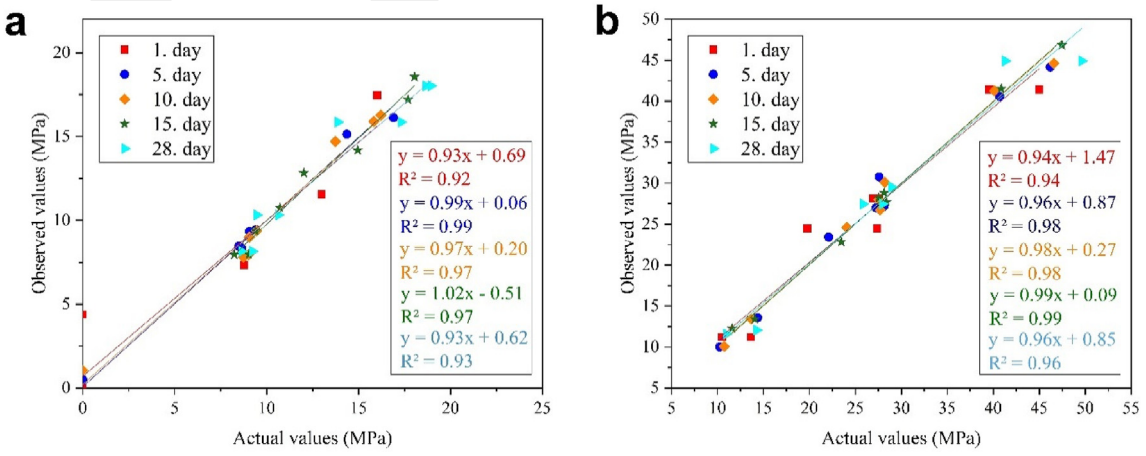

Fig. 4. Actual and predicted UCS values for Yates Analyses from 1st day to 28th day a) with NaOH, b) with Na_2SiO_3.

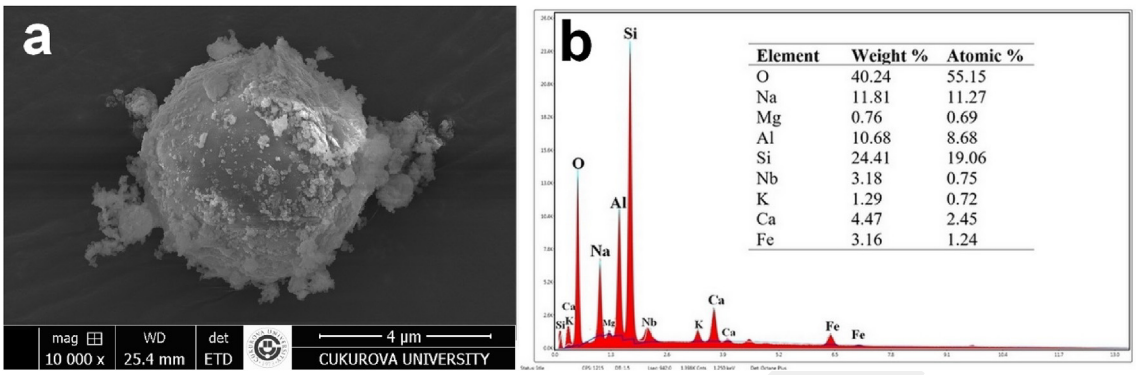

Fig. 5. a) SEM micrograph of geopolymer formation of a fly ash particle and b) EDS spectra.

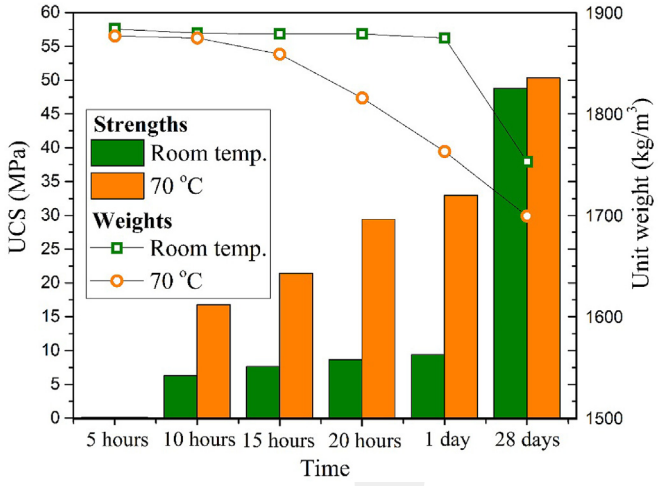

Fig. 6. The UCS value (left) and unit weight (right) of the concretes increases as a function of time at room temperature and 70 °C indicated with green and orange colours, respectively.

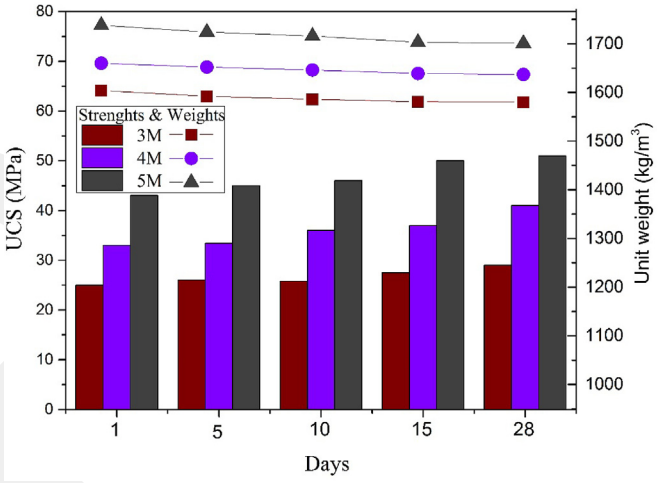

Fig. 7. Effect of Na_2SiO_3 concentration, 3 M (brown), 4 M (purple) and 5 M (dark grey) on the UCS value (left) and unit weight (right) of the concretes as a function of day.

time. These findings are in good agreement with previous studies [52,53]. Although the UCSs obtained at the end of 28 days were close to each other, it was obvious that high strengths were obtained with the effect of high temperature in the early times. It was found that the concrete samples gained 70% of the UCS that was reached at the end of 28 days after 24 h of curing time at 70 °C.

Geopolymer concrete samples were formed using alkaline solutions at a concentration of 3 (brown), 4 (purple) and 5 M (dark grey) to determine the effect of Na_2SiO_3 (see Fig. 7). Increasing the concentration of Na_2SiO_3 led to an increase in the UCS value of the concretes. The concrete specimens were kept in the oven at 70 °C for 1 d and then cured at room temperature. It was detected that the specimens had a 7–8% strength value increase in 28 d compared to 1 d. We observed that while there is an increase in UCSs, the unit weights decreased as a function of day. A 1 M increase in the alkali solution resulted in an extra weight of about 50 kg/m^3. Because alkaline solutions reached saturation and geopolymer concretes were not formed with higher Na_2SiO_3 concentrations.

The optimum conditions were then selected as follows: 5 M Na_2SiO_3 concentration, 70 °C curing temperature, 1 d temperature curing time and 74% solid/liquid ratio that was used in the subsequent tests to prepare lightweight GP concretes by adding lightweight aggregates. In addition, it was targeted to add as much lightweight aggregate as possible to GP concrete specimens for the next tests.

3.3. *Effect of pumice aggregate addition*

The solid/liquid ratio was set at 74%, while the ratio of AP to the amount of fly ash was gradually increased in each experiment. We observed that the workability of the specimens increased within increasing the ratio of AP/fly ash during the sample preparation processes. Fig. 8 shows that the UCS of the concrete decreases within increasing the amount of AP in the specimen. However, a dramatic decrease was observed in the strengths after 15% AP addition. The strengths decreased from 50 MPa to 15 MPa when 200 kg of lightning was achieved.

As seen in Fig. 9 the PLS of the specimens were decreased due to adding pumice in concentration up to 50%. . The PLS presents a similar trent with the UCS value of the specimen.

Applying a point force to the specimens for the point load strength experiment, the tensile strength is actually defeated during this test. Therefore, the point load strength can also be considered as indirect tensile strength. It is normal for point load strengths to be lower than UCSs. Because the UCSs of solid bodies is higher than their tensile strength. Stress-strain curves demonstrated in Fig. 10 showed that the amount of pumice aggregate increased, the strength decreased, and the concrete specimens became more ductile.

As an expected, the WAR value of the concrete increased when adding AP, which has a porous structure, into the mix proportion. The fact that sound waves spent more time in the pores inside AP

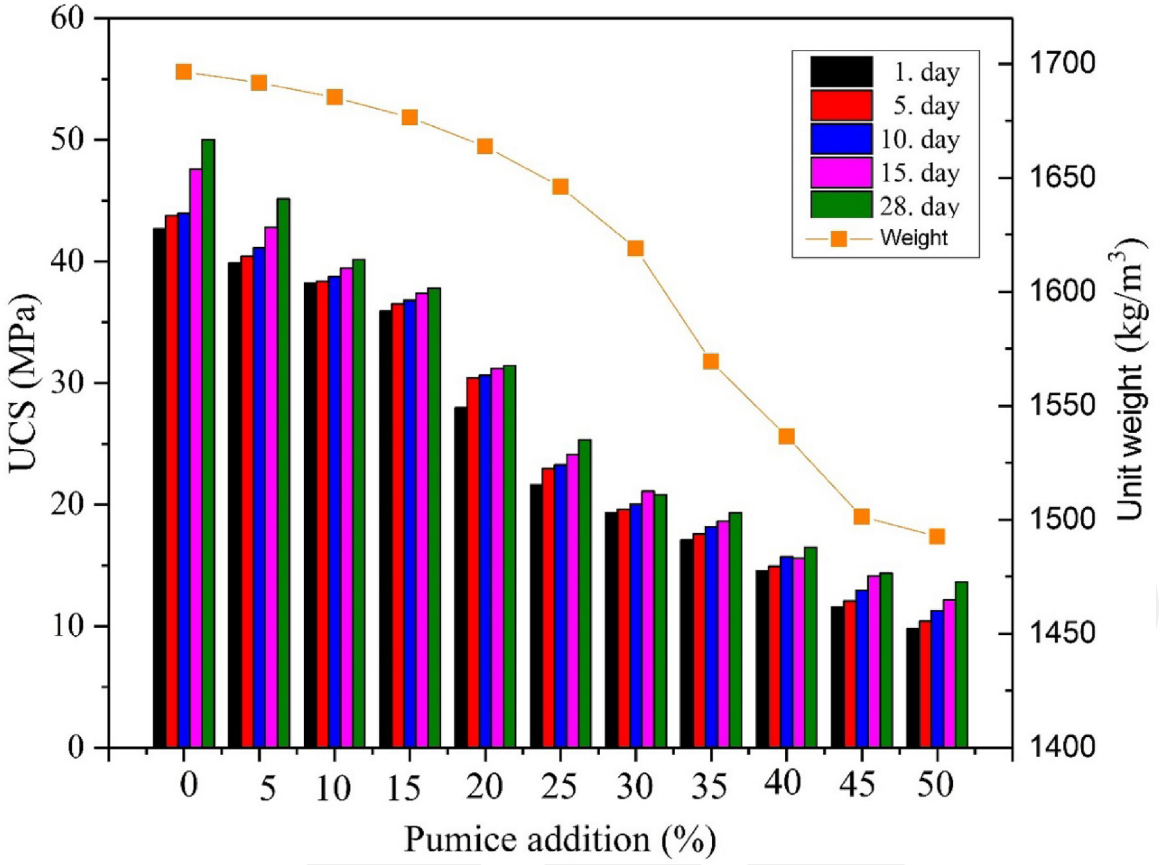

Fig. 8. The UCSs and unit weight of the lightweight GP concrete for given days as a function of pumice addition up to 50%.

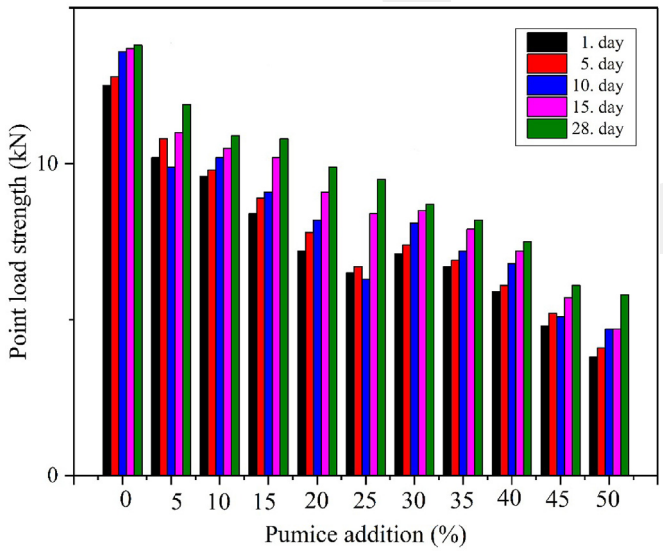

Fig. 9. The point load strength of the lightweight GP concrete with increasing pumice addition up to 50% for given days.

resulted in a reduction in SS values (see Table 4).

The effect of AP's particle size (−0.425 mm, −4+0.425 mm and −12 + 4 mm) on the UCS properties of concrete is listed in Table 5, which gives that an increase in the particle size of AP used as aggregate led to a decrease in the UCS of the concrete. The WAR value of the −0.425 mm AP aggregate containing concrete was

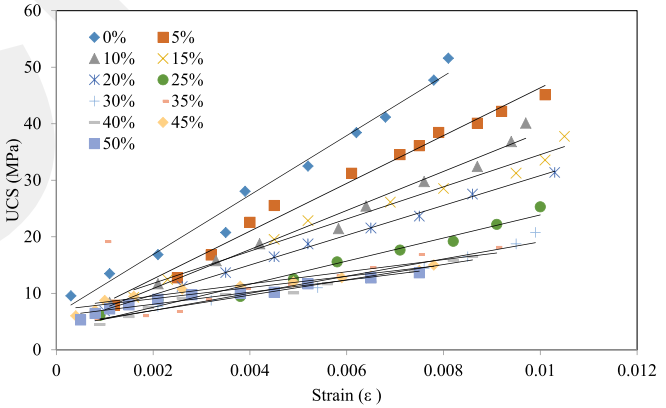

Fig. 10. UCS value plotted as a function of stress-strain for pumice aggregates added specimens (for 28th day).

found to be 3.42%, whereas the concrete containing −12 + 4 mm AP aggregate was prepared with WAR of 6.49%. Moreover, the SS of the concrete was measured to be 2.34, 3.92, and 3.92 km/s respectively (from coarse sized to the finest sized), but there was no remarkable change observed in MH values (~3.5) of the concrete.

3.4. Effect of EP aggregate addition

In order to investigate the effect of particle size, EP aggregates were first divided into −4+0 mm and −0.425 + 0 mm dimensions and added to the mortar formed by using fly ash. The solid/liquid

Table 4
SS, MH and WAR values of the specimens on 28th day.

Pumice (%)	0	5	10	15	20	25	30	35	40	45	50
WAR (%)	1.05	2.25	3.15	3.36	3.21	3.54	3.58	3.61	3.71	3.83	4.59
SS (km/s)	4.12	3.69	3.51	3.50	3.40	3.32	3.28	3.10	2.41	2.25	2.12
MH	5.50	4.50	3.50	3.00	3.00	3.00	2.50	2.50	2.50	2.00	2.00

Table 5
Effect of pumice aggregate sizes on the sample strengths (ratio of AP/fly ash by weight: 20%).

Pumice aggregate size (mm)	UCS (MPa)					Weights (kg/m^3)
	1st d	5th d	10th d	15th d	28th d	
−0.425 + 0	30.00	32.12	33.22	34.25	34.00	1680.81
−4+0.425	28.22	31.12	31.25	32.45	32.23	1644.82
−12 + 4	21.21	21.80	22.50	22.21	24.21	1497.60

ratio was arranged at 73.3%. In addition to having a porous structure like AP, EP had a very low bulk density (0.143 g/cm^3) and the added amount of EP aggregates did not exceed 5% for coarse aggregates (−4+0 mm). While the EP aggregates included in 0.5% ratios by weight, approximately 5 MPa decreases were observed for each adding step (see Fig. 11a). Although the strengths were higher than the −4+0 mm sized aggregate added specimens, there was no decrease in the concrete weights for the specimens produced by fine aggregates in the range of −0.425 + 0 mm (Fig. 11b). Unlike pumice aggregates, which could be added to the mortar at a high rate, the EP aggregates were added at a low rate because of undetectable strengths obtained. To overcome this, EP aggregates were wetted before adding to the mortar. Because EP had hydrophilic nature [54], the alkaline solution was intended to react directly with the fly ash without absorption by the EP aggregates. EP samples were mixed with 0.5 L of tap water for 10 min without grinding medium in the stir ball mill. Subsequently, the materials were sieved through a 425 μm sized sieve and the samples remaining on the sieve were added to the mortar to form GP concrete specimens. It was determined that the mill output coarse EP aggregates absorbed 200% by mass of water. Pre-wetting reduced the alkali solution consumption by 32.5%. Not only the lower chemical consumption was achieved, but also the lowest weighted lightweight GP concretes were produced (see Fig. 11c and d). Some of the broken specimens are shown in Fig. 12.

Table 6 shows the WAR, MH and SS values of the concretes. The

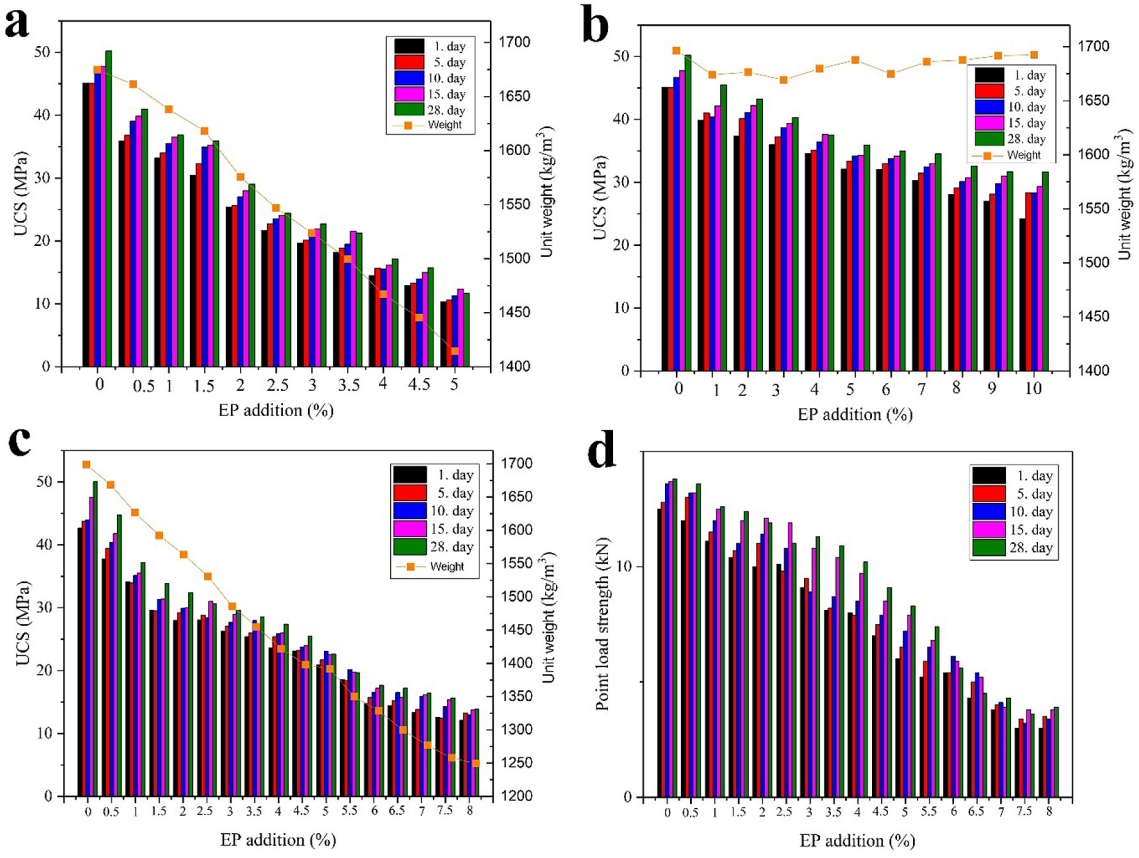

Fig. 11. Effects of different sized EP aggregate addition [a) −4+0 mm, b) −0.425 + 0 mm, c) and d) −4+0.425 mm (with pre-wetting)] on the strengths.

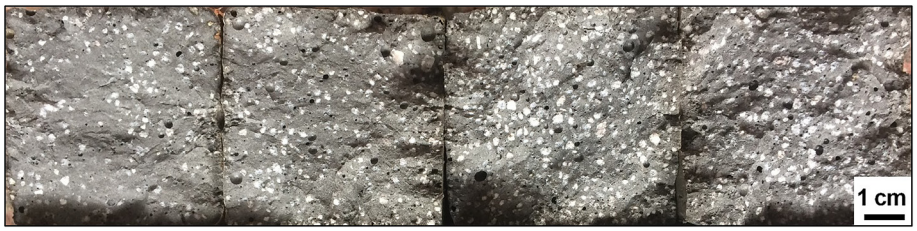

Fig. 12. Broken specimens obtained using pre-wetted EP.

Table 6
MH, SS and WAR values of the concretes on 28th day.

-4+0.425 mm pre-wetted EP addition (%)	WAR (%)	SS (km/s)	MH
0	1.05	4.12	5.5
0.5	1.82	3.32	5.0
1	2.35	3.15	5.0
1.5	4.65	3.00	4.5
2	6.78	2.93	4.5
2.5	9.40	2.91	4.0
3	11.79	2.81	4.0
3.5	12.33	2.69	4.0
4	11.34	2.52	3.5
4.5	13.16	2.45	3.5
5	12.00	2.32	3.5
5.5	14.64	2.05	3.0
6	14.01	1.92	3.0
6.5	14.88	1.83	2.5
7	16.00	1.76	2.5
7.5	17.46	1.72	2.5
8	18.94	1.63	2.5

MH and SS velocity values decreased in parallel with the decreases in strengths while WAR values increased. Adding EP aggregate resulted in more elastic concrete structures. Also, Young modulus of the lightweight concrete specimens declined (Fig. 13).

4. Conclusions

Lightweight concretes offer numerous benefits such as easier transportation, reduced dead load on structural elements, and better fire resistance. In this study, we demonstrated that the lightweight GP concretes could be produced by utilizing the fly ash wastes with lightweight aggregates. The optimum GP concrete preparation parameters were determined by Yates Analysis. The GP concrete production was modelled and formulated. Temperature and alkaline solution concentration were predominant parameters for the geopolymerization process. The GP concrete specimens prepared by Na_2SiO_3 were found to be more durable than the ones produced by NaOH. Therefore, Na_2SiO_3 was chosen as an alkaline activator in the further experiments in which the lightweight AP and EP aggregates were used. The other parameters for optimal geopolymer concrete production were 5 M Na_2SiO_3 concentration, 70 °C curing temperature, 1 d temperature curing time and 74% solid/liquid ratio. Lightweight concretes could be obtained with the addition of up to 50% AP aggregates, and this value did not exceed 10% for EP aggregates. Lighter concretes could be produced by using EP aggregates compared to the AP aggregates. For both aggregate types, the UCSs and unit weights decreased with increasing grain sizes of aggregates. In addition, pre-wetting was applied to the hydrophilic EP aggregates that had the particle size of −4+0.425 mm. In this way, the alkali solution was intended to react with the fly ash undertaking the cement duty instead of EP. All the produced GP concrete specimens were lightweight but the lightest GP concretes (1250 kg/m^3) were obtained by pre-wetting of EP aggregates. Pre-wetting also reduced chemical consumption by 32.5%. Lightweight concrete samples had UCSs between 10 and 50 MPa. SS, PLS, WAR, and MH values are in good agreement with those of UCSs.

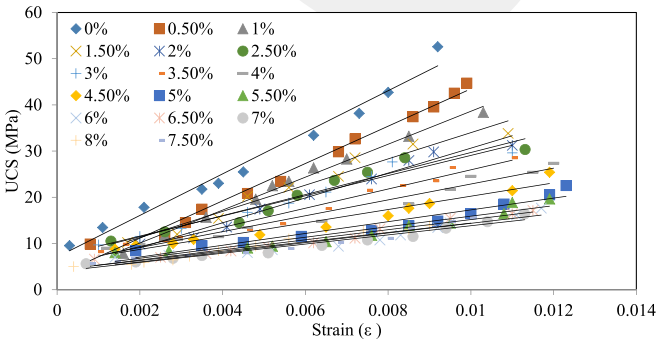

Fig. 13. Stress-strain curves for −4+0.425 mm pre-wetted EP aggregate added specimens (for 28th day).

Acknowledgement

Scientific Research Project Unit of Cukurova University supported this study (Grand number: FBA-2017-8313).

Appendix A. Supplementary data

Supplementary data to this article can be found online at https://doi.org/10.1016/j.molstruc.2019.127236.

References

[1] N.T. Abdel-Ghani, H.A. Elsayed, S. Abdelmoied, Geopolymer synthesis by the alkali-activation of blastfurnace steel slag and its fire-resistance, HBRC. J. 14 (2) (2018) 159–164, https://doi.org/10.1016/j.hbrcj.2016.06.001.
[2] Y. Cheng, M. Hongkiang, C. Hongyu, W. Jiaxin, S. Jing, L. Zonghui, Y. Mingkai, Preparation and characterization of coal gangue geopolymers, Constr. Build. Mater. 187 (2018) 318–326, https://doi.org/10.1016/j.conbuildmat.2018.07.220.
[3] P. Zhang, Y. Zheng, K. Wang, J. Zhang, A review on properties of fresh and hardened geopolymer mortar, Compos. B Eng. 152 (2018) 79–95, https://doi.org/10.1016/j.compositesb.2018.06.031.
[4] W. Shen, L. Cao, Q. Li, W. Zhang, G. Wang, C. Li, Quantifying CO_2 emissions from China's cement industry, Renew. Sustain. Energy Rev. 50 (2015) 1004–1012, https://doi.org/10.1016/j.rser.2015.05.031.
[5] A. Rolfe, Y. Huang, M. Haaf, A. Pita, S. Rezvani, A. Dave, N.J. Hewitt, Technical and environmental study of calcium carbonate looping versus oxy-fuel options for low CO_2 emission cement plants, Int. J. Greenh. Gas Con. 75 (2018) 85–97, https://doi.org/10.1016/j.ijggc.2018.05.020.
[6] R. Maddalena, J.J. Roberts, A. Hamilton, Can Portland cement be replaced by low-carbon alternative materials? A study on the thermal properties and carbon emissions of innovative cements, J. Clean. Prod. 186 (2018) 933–942, https://doi.org/10.1016/j.jclepro.2018.02.138.
[7] Z. Pan, Z. Tao, Y.F. Cao, R. Wuhrer, T. Murphy, Compressive strength and microstructure of alkali-activated fly ash/slag binders at high temperature, Cement Concr. Compos. 86 (2018) 9–18, https://doi.org/10.1016/j.cemconcomp.2017.09.011.
[8] M. Askarian, Z. Tao, G. Adam, B. Samali, Mechanical properties of ambient

cured one-part hybrid OPC-geopolymer concrete, Constr. Build. Mater. 186 (2018) 330–337, https://doi.org/10.1016/j.conbuildmat.2018.07.160.
[9] J. Davidovits, Geopolymers: inorganic polymeric new materials, J. Therm. Anal. 37 (1991) 1633–1656, https://doi.org/10.1007/BF01912193.
[10] M. Sisol, M. Drabova, J. Mosej, Alkali activation of fresh and deposited black coal fly ash with high loss on ignition, Gospod. Surowcami Miner. 30 (2) (2014) 103–115, https://doi.org/10.2478/gospo-2014-0014.
[11] L. Yun-Ming, H. Cheng-Yong, M.M.A. Bakri, K. Hussin, Structure and properties of clay-based geopolymer cements: a review, Prog. Mater. Sci. 83 (2016) 595–629, https://doi.org/10.1016/j.pmatsci.2016.08.002.
[12] V. Nikolic, M. Komljenovic, N. Dzunuzovic, Z. Miladinovic, The influence of Pb addition on the properties of fly ash-based geopolymers, J. Hazard Mater. 350 (2018) 98–107, https://doi.org/10.1016/j.jhazmat.2018.02.023.
[13] T. Bai, Z.G. Song, Y.G. Wu, X.D. Hu, H. Bai, Influence of steel slag on the mechanical properties and curing time of metakaolin geopolymer, Ceram. Int. 44 (2018) 15706–15713, https://doi.org/10.1016/j.ceramint.2018.05.243.
[14] A. Hajimohammadi, T. Ngo, A. Kashani, Glass waste versus sand as aggregates: the characteristics of the evolving geopolymer binders, J. Clean. Prod. 193 (2018) 593–603, https://doi.org/10.1016/j.jclepro.2018.05.086.
[15] G. Ascensao, M.P. Seabra, J.B. Aguiar, J.A. Labrincha, Red mud-based geopolymers with tailored alkali diffusion properties and pH buffering ability, J. Clean. Prod. 148 (2017) 23–30, https://doi.org/10.1016/j.jclepro.2017.01.150.
[16] H.S. Hassan, H.A. Abdel-Gawwad, S.R. Vasquez Garcia, Israde-Alcantara I., Fabrication and characterization of thermally-insulating coconut ash-based geopolymer foam, Waste Manag. 80 (2018) 235–240, https://doi.org/10.1016/j.wasman.2018.09.022.
[17] A. Arulrajah, T.A. Kua, C. Suksiripattanapong, S. Horpibulsuk, J.S. Shen, Compressive strength and microstructural properties of spent coffee grounds-bagasse ash based geopolymers with slag supplements, J. Clean. Prod. 162 (2017) 1491–1501, https://doi.org/10.1016/j.jclepro.2017.06.171.
[18] Y.J. Patel, N. Shah, Enhancement of the properties of ground granulated blast furnace slag based self compacting geopolymer concrete by incorporating rice husk ash, Constr. Build. Mater. 171 (2018) 654–662, https://doi.org/10.1016/j.conbuildmat.2018.03.166.
[19] M.B. Karakoc, I. Turkmen, M.M. Maras, F. Kantarci, R. Demirboga, Sulfate resistance of ferrochrome slag based geopolymer concrete, Ceram. Int. 42 (2016) 1254–1260, https://doi.org/10.1016/j.ceramint.2015.09.058.
[20] A. Vasquez, V. Cardenas, R.A. Robayo, R.M. Gutierrez, Geopolymer based on concrete demolition waste, Adv. Powder Technol. 27 (2016) 1173–1179, https://doi.org/10.1016/j.apt.2016.03.029.
[21] A. Mousa, M. Mahgoub, M. Hussein, Lightweight concrete in America: presence and challenges, Sustain. Prod. Consum. 15 (2018) 131–144, https://doi.org/10.1016/j.spc.2018.06.007.
[22] H. Zhang, S. Hou, J. Ou, Smart aggregates for monitoring stress in structural lightweight concrete, Measurement 122 (2018) 257–263, https://doi.org/10.1016/j.measurement.2018.03.041.
[23] H. Huang, Y. Yuan, W. Zhang, B. Liu, A. Viani, P. Mácová, Microstructure investigation of the interface between lightweight concrete and normal-weight concrete, Mater. Today Commun. (2019), https://doi.org/10.1016/j.mtcomm.2019.100640.
[24] S. Jafari, S.S. Mahini, Lightweight concrete design using gene expression programing, Constr. Build. Mater. 139 (2017) 93–100, https://doi.org/10.1016/j.conbuildmat.2017.01.120.
[25] E. Yasar, C.D. Atis, A. Kilic, High strength lightweight concrete made with ternary mixtures of cement-fly ash-silica fume and scoria as aggregate, Turk. J. Eng. Environ. Sci. 28 (2004) 95–100.
[26] M. Aslam, P. Shafigh, M.A. Nomeli, M.Z. Jumaat, Manufacturing of high-strength lightweight aggregate concrete using blended coarse lightweight aggregates, J. Clean. Prod. 13 (2017) 53–62, https://doi.org/10.1016/j.jobe.2017.07.002.
[27] Y. Zhao, J. Gao, F. Chen, C. Liu, X. Chen, Utilization of waste clay bricks as coarse and fine aggregates for the preparation of lightweight aggregate concrete, J. Clean. Prod. 201 (2018) 706–715, https://doi.org/10.1016/j.jclepro.2018.08.103.
[28] H.A. Mboya, K.N. Njau, A.L. Mrema, C.K. King'ondu, Influence of scoria and pumice on key performance indicators of Portland cement concrete, Constr. Build. Mater. 197 (2019) 444–453, https://doi.org/10.1016/j.conbuildmat.2018.11.228.
[29] A.M. Rashad, Vermiculite as a construction material – a short guide for Civil Engineer, Constr. Build. Mater. 125 (2016) 53–62, https://doi.org/10.1016/j.conbuildmat.2016.08.019.
[30] B. Coppola, L. Courard, F. Michel, L. Incarnato, L.D. Maio, Investigation on the use of foamed plastic waste as natural aggregates replacement in lightweight mortar, Compos. B Eng. 99 (2016) 75–83, https://doi.org/10.1016/j.compositesb.2016.05.058.
[31] B. Ayati, V. Ferrandiz-Mas, D. Newport, C. Cheeseman, Use of clay in the manufacture of lightweight aggregate, Constr. Build. Mater. 162 (2018) 124–131, https://doi.org/10.1016/j.conbuildmat.2017.12.018.
[32] K.H. Mo, H.J. Lee, M.Y.J. Liu, T.C. Ling, Incorporation of expanded vermiculite lightweight aggregate in cement mortar, Constr. Build. Mater. 179 (2018) 302–306, https://doi.org/10.1016/j.conbuildmat.2018.05.219.
[33] J. Castro, L. Keiser, M. Golias, J. Weiss, Absorption and desorption properties of fine lightweight aggregate for application to internally cured concrete mixtures, Cement Concr. Compos. 33 (10) (2011) 1001–1008, https://doi.org/10.1016/j.cemconcomp.2011.07.006.
[34] P. Shafigh, L.J. Chai, H.B. Mahmud, M.A. Nomeli, A comparison study of the fresh and hardened properties of normal weight and lightweight aggregate concretes, J. Build. Eng. 15 (2018) 252–260, https://doi.org/10.1016/j.jobe.2017.11.025.
[35] N. Kabay, F. Aköz, Effect of prewetting methods on some fresh and hardened properties of concrete with pumice aggregate, Cement Concr. Compos. 34 (4) (2012) 503–507, https://doi.org/10.1016/j.cemconcomp.2011.11.022.
[36] D. Shen, J. Jiang, J. Shen, P. Yao, G. Jiang, Influence of prewetted lightweight aggregates on the behavior and cracking potential of internally cured concrete at an early age, Constr. Build. Mater. 99 (2015) 260–271, https://doi.org/10.1016/j.conbuildmat.2015.08.093.
[37] ASTM C618-17a, Standard Specification for Coal Fly Ash and Raw or Calcined Natural Pozzolan for Use in Concrete, ASTM International, West Conshohocken, PA, 2017. www.astm.org.
[38] M. Cabuk, Electrorheological response of mesoporous expanded perlite particles, Microporous Mesoporous Mater. 247 (2017) 60–65, https://doi.org/10.1016/j.micromeso.2017.03.044.
[39] X. Li, H. Chen, L. Liu, Z. Lu, J.G. Sanjayan, W.H. Duan, Development of granular expanded perlite/paraffin phase change material composites and prevention of leakage, Sol. Energy 137 (2016) 179–188, https://doi.org/10.1016/j.solener.2016.08.012.
[40] M.F. Granata, Pumice powder as filler of self-compacting concrete, Constr. Build. Mater. 96 (2015) 581–590, https://doi.org/10.1016/j.conbuildmat.2015.08.040.
[41] B. Ersoy, A. Sariisik, S. Dikmen, G. Sariisik, Characterization of acidic pumice and determination of its electrokinetic properties in water, Powder Technol. 197 (2010) 129–135, https://doi.org/10.1016/j.powtec.2009.09.005.
[42] TS 802, Design Concrete Mixes, Turkish Standard, 2016.
[43] ASTM C109/C109M-16a, Standard Test Method for Compressive Strength of Hydraulic Cement Mortars (Using 2-in. Or [50-mm] Cube Specimens), ASTM International, West Conshohocken, PA, 2016. www.astm.org.
[44] ASTM C1245/C1245M-12, Standard Test Method for Determining Relative Bond Strength between Hardened Roller Compacted Concrete Lifts (Point Load Test), ASTM International, West Conshohocken, PA, 2012. www.astm.org.
[45] ASTM C642-13, Standard Test Method for Density, Absorption, and Voids in Hardened Concrete, ASTM International, West Conshohocken, PA, 2013. www.astm.org.
[46] ASTM C597-16, Standard Test Method for Pulse Velocity through Concrete, ASTM International, West Conshohocken, PA, 2016. www.astm.org.
[47] M. Závacký, J. Štefaňák, V. Horák, L. Miča, Statistical estimate of uniaxial compressive strength of rock based on shore hardness, Procedia Eng. 191 (2017) 248–255, https://doi.org/10.1016/j.proeng.2017.05.178.
[48] E. Yogurtcuoglu, M. Ucurum, Surface modification of calcite by wet-stirred ball milling and its properties, Powder Technol. 214 (2011) 47–53, https://doi.org/10.1016/j.powtec.2011.07.032.
[49] O.Y. Toraman, D. Katircioglu, A study on the effect of process parameters in stirred ball mill, Adv. Powder Technol. 22 (2011) 26, https://doi.org/10.1016/j.apt.2010.02.018.
[50] Z. Yahya, M.M.A.B. Abdullah, K. Hussin, K.N. Ismail, R.A. Razak, A.V. Sandu, Effect of solids-to-liquids, Na_2SiO_3-to-NaOH and curing temperature on the palm oil boiler ash (Si + Ca) geopolymerisation system, Materials 8 (2015) 2227–2242, https://doi.org/10.3390/ma8052227.
[51] H. Xu, J.S.J. Van Deventer, The geopolymerisation of alumino-silicate minerals, Int. J. Miner. Process. 59 (2000) 247–266, https://doi.org/10.1016/S0301-7516(99)00074-5.
[52] B. Mo, H. Zhu, X. Cui, Y. He, S. Gong, Effect of curing temperature on geopolymerization of metakaolin-based geopolymers, Appl. Clay Sci. 99 (2014) 144–148, https://doi.org/10.1016/j.clay.2014.06.024.
[53] A.A. Adam, X.X.X. Horianto, The effect of temperature and duration of curing on the strength of fly ash based geopolymer mortar, Procedia Eng. 95 (2014) 410–414, https://doi.org/10.1016/j.proeng.2014.12.199.
[54] M. Gursoy, M. Karaman, Improvement of wetting properties of expanded perlite particles by an organic conformal coating, Prog. Org. Coat. 120 (2018) 190–197, https://doi.org/10.1016/j.porgcoat.2018.03.021.